

Compression of a cold atomic cloud by on-resonance laser light

Lev Khaykovich and Nir Davidson

Department of Physics of Complex Systems, Weizmann Institute of Science, Rehovot 76100, Israel

Received September 16, 1998; revised manuscript received February 16, 1999

We analyze the light-induced atom-atom interactions in optically thick atomic clouds and show that, when the laser frequency is on-resonance with the atomic transition, they become attractive. On the basis of this analysis we propose and demonstrate a novel scheme to compress a cold and dense atomic cloud with a short on-resonance laser pulse. The compression force arises from attenuation of the laser light by the atomic cloud. The following free propagation of the atoms shows a lenslike behavior that yields a transient density increase at the focal time, where neither laser nor magnetic field perturbations exist. A cooling pulse, which is applied at the focal time of this lens, restores the initial temperature of atoms, and hence the phase space density is increased. Finally, we adopt our compression scheme to a quasi-steady-state mode by temporally chopping it with the cooling and trapping beams of a magnet-optical trap. © 1999 Optical Society of America
[S0740-3224(99)01905-0]

OCIS codes: 140.3320, 140.7010.

1. INTRODUCTION

The ability to capture, cool, and store atoms in a magneto-optical trap¹ (MOT) has stimulated a broad field of research in atomic physics and quantum optics.² The MOT typically yields densities of the order of $\sim 10^{11}$ atoms/cm³ and temperatures of the order of 50 μ K. For many experiments, in particular those involving cold collisions and quantum statistics effects, higher trapped-atom densities are needed. This need stimulated many studies of the physical mechanisms that limit the trapped-atom densities and of ways to overcome them.

For small numbers of trapped atoms the MOT can be accurately described according to a single-atom picture, where the light forces define the temperature and the spring constant of the trap, which determine its density. As the number of trapped atoms increases, light-induced atom-atom interactions become important.³ These repulsive interactions arise by reabsorption of spontaneously scattered photons (radiation trapping), where photon momentum exchange between the atoms pushes them apart. An additional effective interaction between the atoms arises owing to attenuation of the laser beams by the atomic cloud. These laser-attenuation effects were discussed theoretically for clouds with both small⁴ and arbitrary⁵ optical thickness. They were shown to induce an attractive atom-atom interaction that tends to compress the atoms. Unfortunately, under typical MOT conditions the repulsive interactions are stronger than the attractive ones, and their net result is an upper limit on the density.³

The steady-state density is determined by a balance between the spring constant of the trap and the repulsive atom-atom interactions.³ One can therefore increase it either by increasing the spring constant or by suppressing the atom-atom interactions. One can obtain an increased spring constant by increasing the magnetic-field gradient of the MOT.⁶ Since strong field gradients im-

pede the loading rate of atoms into the MOT, they were only applied transiently.

Suppression of atom-atom interactions was achieved by two methods. In the first method, known as a dark MOT,⁷ the atoms are confined mainly in a dark hyperfine ground state, which does not interact with the trapping light, and thus they almost do not repel each other. Both a spatial and a temporal version of the dark MOT method were demonstrated as yielding comparable performances.^{7,8} A second method one can use to suppress the atom-atom interaction is by reducing the intensity of the trapping light and/or increasing its detuning, again decreasing the scattering rate of photons.^{9,10}

Finally, in magnetic traps and far-detuned optical dipole traps, where scattering rates of photons are negligible, atom-atom interactions are much smaller and at densities of $\sim 10^{12}$ atoms/cm³ atoms behave nearly according to a single-atom picture. Under such conditions compression can be simply obtained by cooling.¹¹

In this paper we analyze the light-induced atom-atom interactions in optically thick atomic clouds. We show that when the laser frequency is on-resonance with the atomic transition the forces that arise from these interactions change their sign and become attractive. We calculate these forces as a function of the laser beam's intensity and detuning and the atomic-density distribution and show that compression of the atomic cloud and large density increase are possible. We propose a transient scheme to realize such compression, using a short on-resonance pulse of the laser light and demonstrate it using either one, two, or six compression beams on rubidium atoms that are released from a MOT. Finally, we demonstrate how these transient compression schemes can be combined with cooling to obtain not only a density increase but also a net increase in the phase-space density.

Townsend *et al.*⁹ suggested that a density increase may take place during steady-state MOT operation when the

frequency of the trapping laser is tuned close to the atomic resonance, but they did not observe it experimentally. Since our scheme is transient, we could tune the laser frequency exactly on-resonance and also turn off the MOT nonuniform magnetic field to create the necessary conditions for compression.

2. ATTRACTIVE AND REPULSIVE LIGHT-INDUCED FORCES

For a qualitative analysis of the light-induced atom-atom interaction we consider first an optically thin cloud of two-level atoms (where multiple scattering of photons can be neglected), illuminated by a single laser plane wave of intensity I . When coherences, population trapping, and Doppler shifts are neglected, the repulsive force between the atoms owing to reabsorption of scattered photons obeys the relation³ $\nabla \cdot \mathbf{F}_R = \langle \sigma_R \rangle \langle \sigma_L \rangle I n / c$, where n is the atomic density and c is the speed of light. $\langle \sigma_R \rangle$ and $\langle \sigma_L \rangle$ are the average cross sections for absorbing scattered photons and incident laser photons, respectively. Similarly, the attractive force that arises from laser-beam attenuation inside the atomic cloud obeys the relation³ $\nabla \cdot \mathbf{F}_A = -\langle \sigma_L \rangle^2 I n / c$. Therefore the sign of $\langle \sigma_R \rangle / \langle \sigma_L \rangle - 1$ determines the sign of the total atom-atom interaction. For typical steady-state MOT parameters, $\langle \sigma_R \rangle / \langle \sigma_L \rangle - 1$ is positive owing to ac Stark shifts,¹² and therefore the maximum density is limited by this radiation-trapping effect.^{3,9}

This picture can be inverted by bringing the laser frequency exactly on resonance with the atoms. In this case the weak-probe absorption profile takes on negative values,¹³ and the atomic cloud becomes more transparent for reradiated photons than for the incident laser photons. This effect mostly occurs at high laser intensities ($I > I_{\text{sat}}$, where I_{sat} is the saturation intensity of Rb¹⁴). The calculated dependence of $\langle \sigma_R \rangle / \langle \sigma_L \rangle - 1$ on laser intensity for different detunings δ of the laser frequency from resonance is shown in Fig. 1. Two configurations

are presented for each detuning: a plane wave (solid curve in Fig. 1), and average cross sections for a standing wave (dashed curves in Fig. 1). While some differences exist between the results for the two configurations, they are not significant for our analysis. For the plane-wave case, $\langle \sigma_R \rangle$ is calculated by the integral

$$\langle \sigma_R \rangle = \int \sigma(\nu) F(\nu) d\nu, \quad (1)$$

where $F(\nu)$ is the fluorescence spectrum¹² and $\sigma(\nu)$ is the absorption spectrum,¹³ both in the presence of a strong pump. The standing-wave case is complicated by the fact that different atoms are subjected to different pump intensities and hence have distinguished absorption and fluorescence spectra. Since the typical distance for a scattered photon to be absorbed is much larger than the period of a standing wave, we can neglect any correlation between the location of the scattering atom and that of the absorbing atom. We therefore use Eq. (1) to calculate $\langle \sigma_R \rangle$ (and similarly for $\langle \sigma_L \rangle$), where $F(\nu)$ and $\sigma(\nu)$ are now the averaged fluorescence and absorption spectra, respectively.¹⁵

The first curve in Fig. 1, of $\delta = -1.5\gamma$ (γ is the atomic-transition linewidth), shows the case of typical steady-state MOT operation. It indicates repulsive forces between the atoms for all intensities. The second curve, with $\delta = -\gamma$, is close to the border between attractive and repulsive interactions. For the third curve, with $\delta = 0$, $\langle \sigma_R \rangle / \langle \sigma_L \rangle - 1$ is negative for all intensities, and strong compression should be obtained. Note that at $\delta = 0$ laser cooling and magneto-optics trapping are no longer effective, so the compression has to be performed transiently.

When the optical thickness of the atomic cloud is large, the laser-beam intensity is considerably attenuated during its passage through the cloud, and the small-absorption approximation that was used above is no longer valid. We therefore calculate numerically the position and time-dependent attractive (compression) force under realistic assumptions. In particular, we are interested in deviations of the force from a linear dependence on distance, which can be viewed as aberrations from an ideal focusing lens.

Another complication of the optically thick cloud is that multiple scattering of photons leads to strong radiation trapping.¹⁶ This may increase the light-induced repulsive forces beyond the optically thin case treated above. In our model we nevertheless neglect repulsion forces altogether. This is a good assumption for relatively high laser intensities (where $\langle \sigma_R \rangle \ll \langle \sigma_L \rangle$; see Fig. 1) and for not too high optical thickness (where the enhancement of repulsive forces owing to multiple scattering is small).

The average scattering force for an on-resonance ($\delta = 0$) laser plane wave propagating along the x direction is given by

$$\langle F(x, t) \rangle = 1/2 \hbar k \gamma \frac{s(x, t)}{s(x, t) + 1}, \quad (2)$$

where

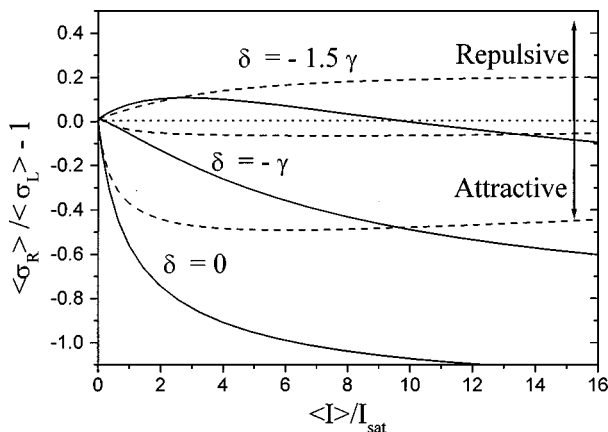


Fig. 1. Average absorption cross sections of rescattered photons ($\langle \sigma_R \rangle$) and laser photons ($\langle \sigma_L \rangle$) calculated for a two-level atom in a plane wave (solid curves) and a standing wave (dashed curves) as a function of average laser intensity for three different laser detunings. Above $\langle \sigma_R \rangle / \langle \sigma_L \rangle - 1 = 0$ there is a repulsive regime, which applies for typical MOT parameters, and below it there is an attractive regime where our experiments were performed.

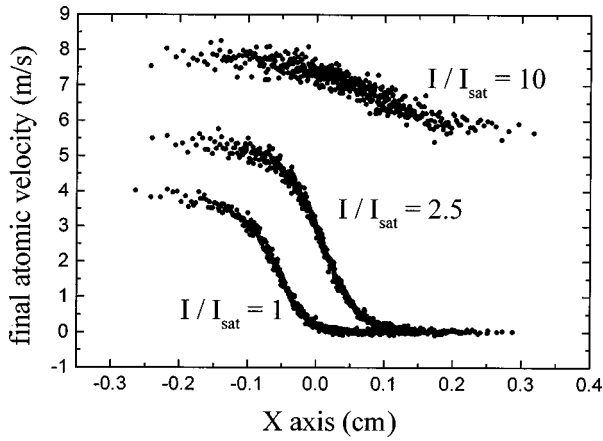


Fig. 2. Distribution of calculated velocities of atoms as a function of position inside a 1-D atomic cloud [an initial $1/e$ diameter of 0.27 cm and optical thickness of $\exp(-11)$] immediately after a 100- μs compression pulse for three incoming laser intensities. Spherical aberration is manifested by the amount of distortion from the general linear slope to the velocity curves, and heating is manifested by the noiselike fluctuations.

$$s(x, t) = \frac{I(x, t)/I_{\text{sat}}}{1 + 4(k\nu(x, t)/\gamma)^2}$$

is the saturation parameter and $\nu(x, t)$ is the atomic velocity. $I(x, t)$ is the light intensity, which obeys the following equation:

$$\frac{1}{I(x, t)} \frac{dI(x, t)}{dx} = \frac{2\langle\sigma_L^0\rangle \int_{-\infty}^x n(x', t) dx'}{1 + I(x, t)/I_{\text{sat}} + 4[k\nu(x, t)/\gamma]^2}, \quad (3)$$

where $\langle\sigma_L^0\rangle = 1.66\lambda^2/2\pi$ is the weak-probe absorption cross section for the linearly polarized laser photons¹⁴ and $n(x, t)$ is the one-dimensional (1-D) atomic-density distribution. We limit ourselves to short laser pulses so that the Doppler shift induced by the final velocities is smaller than $\sim\gamma$ for most atoms. According to Fig. 1 this ensures that the condition $\langle\sigma_R\rangle/\langle\sigma_L\rangle - 1 < 0$ remains valid throughout most of the compression pulse. We numerically integrate the equations of motion for the atoms, using Eqs. (2) and (3) over the pulse duration T and find the final velocity $\nu_f(x_f, T)$ and spatial distributions of the atoms. Note that Eq. (3) has to be integrated again for each time step, because it contains $\nu(x, t)$ and $n(x, t)$, which change in time. We also include the effects of initial temperature and of heating by the fluctuations of the scattering force in a Monte Carlo approach.

In Fig. 2, 1-D atomic-velocity distributions immediately after a 100- μs compression pulse are shown as a function of position in the cloud for three incoming laser intensities: I/I_{sat} equal to 1, 2.5, and 10. The general linear slopes to the curves represent ideal (infinite) compression, where their inverse estimates the focal time T_{focus} where maximal compression is expected. The initial 1-D density distribution was Gaussian with $1/e$ diameter of 0.27 cm, a temperature of 13 μK , and a weak-probe absorption of $\exp(-11)$, as measured in the cloud center of our experiment. For $I/I_{\text{sat}} = 1$ the laser intensity is attenu-

ated rapidly and nearly half of the atoms do not feel any force, so good compression is not expected. For $I/I_{\text{sat}} = 2.5$ (the middle curve in Fig. 2) the absorption distance of the laser beam is comparable to the size of the atomic cloud, resulting in approximately linear dependence of the final velocities on propagation distance, and large compression is therefore expected. For $I/I_{\text{sat}} = 10$ the velocity distribution also has approximately linear dependence on position, but velocity fluctuations owing to heating $\delta\nu_{\text{heat}}$ are larger. Also, T_{focus} is much larger than for $I/I_{\text{sat}} = 2.5$ so the heating contribution to the compressed cloud size $\sim\delta\nu_{\text{heat}}T_{\text{focus}}$ is even further increased.

In Fig. 3 the atomic trajectories are presented as a function of time, after a 100- μs compression pulse with optimal intensity was applied. After focal time $T_{\text{focus}} \sim 600 \mu\text{s}$ the maximal compression is obtained. The spherical aberration is seen from the difference in the focal position of the atomic trajectories. Additional sources of aberrations are the initial temperature of the atoms and heating that is due to the compression pulse.

We calculated the maximal density compression ratio C and the focal time T_{focus} by direct integration of the free space propagation of the atoms after the compression pulse. The maximal compression ratio of ~ 7 is obtained at $I/I_{\text{sat}} = 2.5$ for the atomic cloud with parameters described above. The reduction in C for larger and smaller intensities is expected from the discussion of Fig. 2.¹⁷ If the heating that is due to the compression pulse is omitted from the simulation, C slightly increases to ~ 8 at $I/I_{\text{sat}} = 2.5$, but the decrease of C at higher pulse intensities is much slower. The initial temperature effects on C for typical molasses temperatures are negligibly small.

In our experiments we apply a compression pulse on an atomic cloud with 3-D Gaussian density distribution $n(x, y, z)$, whose optical thickness is proportional to $\int n(x, y, z) dx$ and therefore is also Gaussian. Since the maximal compression ratio, the optimal pulse intensity, and T_{focus} all depend strongly on the optical thickness, they vary across the transverse directions and reduce the average density compression as compared with the 1-D cloud. Figure 4 presents the averaged compression ratio C_{average} ¹⁸ as a function of laser intensity (solid curve; the

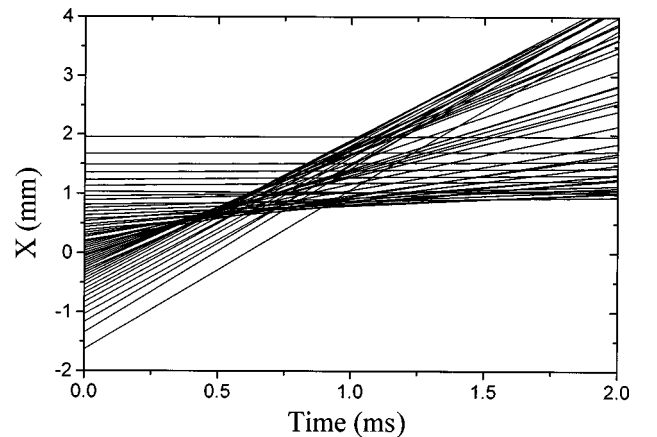


Fig. 3. Atomic trajectories as a function of time are shown, after a 100- μs compression pulse with optimal intensity was applied to an atomic cloud with a Gaussian initial distribution. A maximal compression is observed at $T_{\text{focus}} \sim 600 \mu\text{s}$.

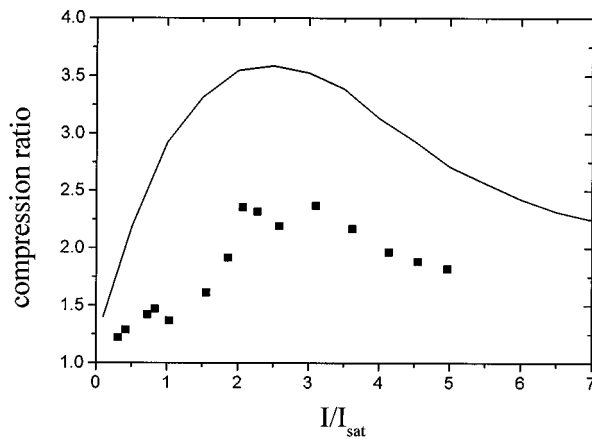


Fig. 4. Calculated dependence of the average compression ratio for a 3-D atomic cloud¹⁸ on incoming laser intensity. The cloud $1/e$ diameter is 0.27 cm, the maximal optical thickness is $\exp(-11)$, and the compression-pulse duration is 100 μs . The scatter graph shows experimental measurements in the one-beam configuration. Each data point is taken at T_{focus} , which is different for each intensity.

experimental points in the figure are discussed below). The maximal C_{average} is ~ 2 times smaller than C for the 1-D cloud and has a similar dependence on the compression-pulse intensity.

3. EXPERIMENTAL RESULTS FOR PULSE COMPRESSION

Our compression experiments consisted of five stages. The first, second, and third stages prepared the cold and optically dense atomic cloud, while optimizing the number, density, and temperature of the atoms, respectively. The fourth stage was the pulse compression, and the fifth stage was detection. A schematic diagram showing our experimental setup is presented in Fig. 5.

In the first stage ⁸⁵Rb atoms were loaded from the vapor cell (vapor pressure of $\sim 3 \times 10^{-9}$ torr) into a MOT. During 500 ms, $\sim 4 \times 10^8$ atoms were captured and cooled. The MOT was composed of three orthogonal beams emerging from a frequency-stabilized Ti:sapphire laser ($1/e$ diameter of 2.1 cm) retroreflected with a cats-eye configuration. The intensity of each beam was 10 mW/cm², and the laser frequency was detuned -17 MHz from the rubidium $5S_{1/2}, F = 3 \rightarrow 6P_{3/2}, F = 4$ line. A 12-mW diode laser locked to the $5S_{1/2}, F = 2 \rightarrow 6P_{3/2}, F = 3$ line of rubidium was used as a source of the repumping light. The magnetic quadrupole field was supplied by an anti-Helmholtz configuration with a field gradient of 6 G/cm, and stray magnetic fields were compensated by three orthogonal Helmholtz coils.

In the second stage, we increased the density of the trapped atoms by decreasing the trapping-beam intensity to 1.5 mW/cm², increasing their detuning to -30 MHz, and also by applying the temporal dark MOT scheme.^{7,8} By detuning the repumping laser by approximately -150 MHz from the $5S_{1/2}, F = 2 \rightarrow 6P_{3/2}, F = 3$ line, we reduced the bright ($F = 3$) ground-state fraction to $p \sim 0.2$. After 30 ms of the weak and dark MOT stage the atomic-cloud density was increased to a nearly isotropic Gaussian shape with a $1/e$ diameter of 0.27 cm (measured

in all three dimensions with calibrated CCD cameras and an image-processing unit), without any loss of atoms. The resulting peak density of $\sim 3 \times 10^{10}$ atoms/cm³ was also verified by a probe absorption measurement with an accuracy of $\sim 20\%$. The optical transmission of the trap for a weak, linearly polarized and on-resonance probe was $\exp(-11)$. We determined the on-resonance optical transmission by fitting the theoretical weak-probe absorption spectrum to a measured one, as in Ref. 7.

In the third and final preparation stage, the magnetic field was shut down (within less than 500 μs), and the atoms were further cooled for 3 ms with polarization-gradient cooling.¹⁹ A final temperature of 13 μK was measured with a time-of-flight technique, without any density decrease.

The pulse compression was performed next, after a delay of 200 μs . The atoms were illuminated from above for 100 μs by an additional, linearly polarized laser beam on-resonance with atomic transition and $I = 7.5$ mW/cm². The size of the beam (1.4-cm $1/e$ diameter) was much larger than the atomic cloud, so the atoms felt a nearly uniform intensity. After a variable delay the MOT beams were turned on for 100 μs , and the fluorescence signal was imaged to the CCD camera (looking from the side) that measured the size of the atomic cloud and also the peak atomic 1-D integrated density.¹⁸

Figure 6 shows the atomic 1-D integrated density profile (the central scan of the CCD fluorescence image) as a function of the delay between the compression and the detection pulses. As seen, the atomic density first increases as the atoms are compressed, reaches a maximum at $T_{\text{focus}} = 700$ μs , and then decreases. The width of the atomic cloud decreases as the peak intensity increases, to reach a minimum at T_{focus} . The shape of the cloud significantly distorts only at times longer than T_{focus} .

We repeated the experiment with different intensities and durations of the compression pulse, and we measured T_{focus} for each case and the compression of the atomic density at T_{focus} . The results for that maximal compression are shown in Fig. 4 together with the theoretical prediction that is presented above. As seen, the experiment reveals the same trend as theory, namely, the existence of an optimal intensity for the compression pulse, with good agreement for the value of that optimum. However, the maximal theoretical compression is ~ 3.5 , while in the experiment we obtained compression of only ~ 2.2 . We at-

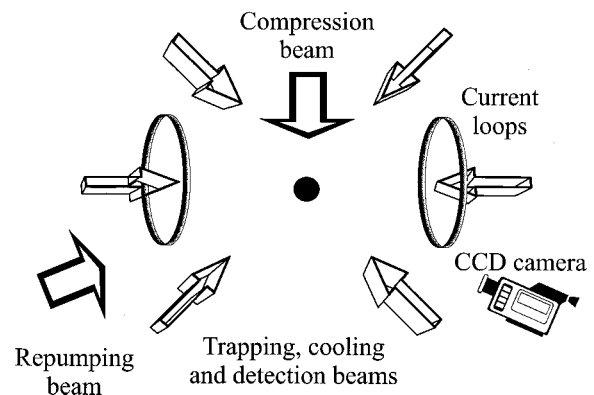


Fig. 5. Schematic diagram of our experimental setup.

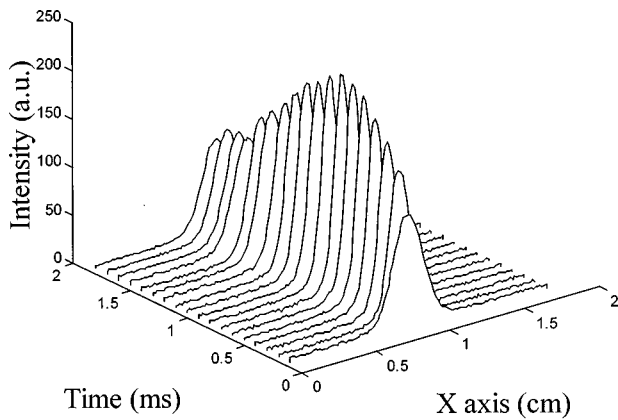


Fig. 6. Time developments of the 1-D integrated density profile (the central line scan of the CCD fluorescence image) of the atomic cloud after the compression pulse is switched off. At $T_{\text{focus}} = 700 \mu\text{s}$ the peak reaches its maximum and then decreases, while the width of the atomic cloud minimizes at T_{focus} .

tribute this reduction to repulsive-force action at low intensities, in particular at the last stages of the compression pulse where the Doppler shifts approach γ . For our experimental parameters, the probability of reabsorbing a scattered photon is larger than 0.5 for $I < 2I_{\text{sat}}$. Therefore we expect that multiple scattering at that regime even further enhances repulsive forces, and their neglect in the model is even less justified.

We also checked the sensitivity of the focal time and the maximal compression to other experimental parameters. First, we found that the compression ratio is relatively insensitive to the duration of the compression pulse, yielding nearly optimal compression over the range 30–200 μs . The focal time did depend on the pulse duration and increased as the latter decreased, as was also confirmed by our calculations. At pulse durations shorter than 30 μs the focal time is long enough for the maximal compression to degrade because of the initial temperature of atoms. When the pulse duration was $>200 \mu\text{s}$ the focusing occurred during the compression pulse and thus prevented its measurement.

Second, to verify that the compression we observed is related to optical thickness of the atomic cloud, we decreased the number of atoms in the MOT by ~ 1000 (to $\sim 5 \times 10^5$). The resulting optical density of the atomic cloud reduced to 1.6, and the compression effect almost disappeared (maximal compression ratio ~ 1.1), while the laser intensity that maximized compression also reduced (from $2.5I_{\text{sat}}$ to $0.5I_{\text{sat}}$), in agreement with our calculations. The reduction in the optimal laser intensity for small optical densities is expected by the arguments of Section 2 and is also predicted by our numerical calculations. The reduction of the maximal compression ratio therefore results from the large repulsive forces that exist for these small laser intensities (see Fig. 1).

Third, we measured the dependence of the maximal compression as a function of compression-pulse frequency detuning. This dependence is shown as an inset in Fig. 7²⁰ and is in agreement with the theoretical model of Fig. 1, which predicts that for detunings larger than $\sim \gamma$ the net light-induced interaction between the atoms is repulsive.

The one-beam compression scheme was inherently asymmetric and indeed tended to distort the MOT at long delay times. To prevent such distortions and to improve the compression ratio, we retroreflected the compression beam so as to illuminate the atoms from the opposite direction. A small misalignment of the retroreflected beam prevented it from being largely attenuated by its first pass through the atomic cloud. This two-beam configuration yielded an improved maximal compression of ~ 3.5 (as opposed to ~ 2.2 for the one-beam case) and also caused less distortions of the atomic cloud. Otherwise, the two-beam configuration behaved in a way similar to the one-beam configuration and showed similar dependence on total beam intensity, detuning, and pulse duration. We applied our simulations to the two-beam configuration and found a factor of ~ 2 increase in the maximal compression ratio over the one-beam configuration ($C_{\text{max}} = 8$ instead of 3.5). However, since the two-beam configuration involves multi-photon transitions, which are not included in our theoretical model, such an agreement may be accidental. The simulations neglect the standing-wave pattern but include mutual influence between the two beams through saturation of atoms. We did this by solving Eq. (3) for each beam in iterations, while replacing $I(x, t)$ on the right side of the equation by $I_1(x, t) + I_2(x, t)$. The iterations were repeated until a self-consistent solution was found for both $I_1(x, t)$ and $I_2(x, t)$.

Finally, we utilized our compression scheme in a three-dimensional (3-D) configuration to receive high 3-D densities in the atomic cloud. The same six beams that were used for the MOT in this case provided the compression pulse. Again, we observed the fluorescence induced by the detection pulse with two CCD cameras located at orthogonal directions to determine the size of the atomic cloud in all three dimensions (which was found to be nearly uniform) and also its 3-D density. The increase in 3-D density of atoms in the compressed cloud was derived from the ratio of the peak fluorescence and the size measurements and is defined as the 3-D compression ratio. In Fig. 7 the dependence of compression on the average

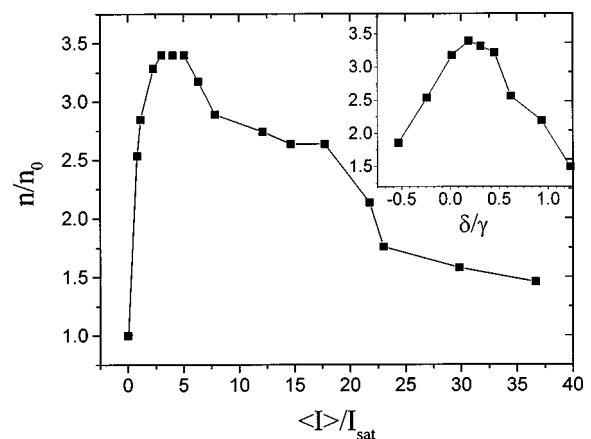


Fig. 7. Peak density compression ratio in the six-beam configuration with $\delta = 0$ as a function of average laser intensity. The symbols are our experimental data, and the connecting lines are only to guide the eye. The inset shows the dependence of the compression ratio on detuning of the laser frequency from resonance at $\langle I \rangle / I_{\text{sat}} = 4$.

laser intensity for a 100- μ s compression pulse is shown. As seen, it is qualitatively similar to that of the 1-D case yielding a maximal compression of ~ 3.5 for the optimal average intensity of 12 mW/cm². Our best results, with compression of 4, were obtained with a 170- μ s pulse duration, yielding a final atomic density of $\sim 1.2 \times 10^{11}$ atoms/cm³, which is comparable with other schemes to increase density, such as increasing the magnetic field. That optimal intensity is ~ 2 times larger than for the 1-D case. Part of that factor can be attributed to the lack of average optical pumping in the complicated interference pattern of the six beams, which would tend to increase I_{sat} .¹⁴ As for the two-beam configuration, the six-beam configuration is potentially more complex than the one-beam configuration, and direct comparison with theory is not straightforward.

4. COMBINING COOLING WITH COMPRESSION

The increase in density in our compression scheme is expressed at the expense of heating. In order to increase the phase-space density we utilized a cooling of atoms when they approach the center of the atomic cloud at T_{focus} . The cooling pulse, which was produced by red-detuned MOT beams ($\delta = -30$ MHz), was applied at T_{focus} of the two-beam compression scheme. It consisted of two parts: the first one was optimized for Doppler cooling with a high-velocity capture range ($I = 20$ mW/cm²), and the second one with reduced intensity ($I = 3$ mW/cm²) significantly decreased the temperature of atoms owing to the polarization-gradient cooling scheme. In Fig. 8 we show the time development of the cloud size with and without a cooling pulse. The compression pulse was 50 μ s long, while Doppler cooling was 200 μ s long and the polarization gradient was 100 μ s. We found that under these conditions the cooling at the focus can restore the initial temperature of atoms, and therefore the phase-space density increased by the same amount as the density ($\sim 3\times$ in this case).

For a quasi-steady-state operation we also investigated a combination of (on-resonance) compression pulses with the cooling and trapping (off-resonance) MOT beams. First, we tried to add the compression beams (either one, two, or six beams) continuously in addition to MOT beams. No compression was observed for a wide range of MOT and compression-beam parameters. Next, we chopped the MOT and compression beams so they would not illuminate the atoms simultaneously. The peak density was measured, as in the pulsed compression experiments, by the image of the fluorescence induced by a probe pulse. Best compression was obtained for chopping cycles of 200 μ s that included 180 μ s of MOT beams (at $I = 10$ mW/cm² and $\delta = -17$ MHz) and 20 μ s of compression beams (at $I = 1.1$ mW/cm² per beam and $\delta = 0$). For compression to MOT times ratio larger than ~ 0.2 a substantial reduction in the number of atoms was observed. The peak density as a function of compression-beam detuning is shown in Fig. 9 for two counterpropagating compression beams. As seen, the maximal (quasi) steady-state compression was $C = 1.6$. The existence of a maximum at exactly $\delta = 0$ is a clear evidence of the attenuation-induced compression.²¹

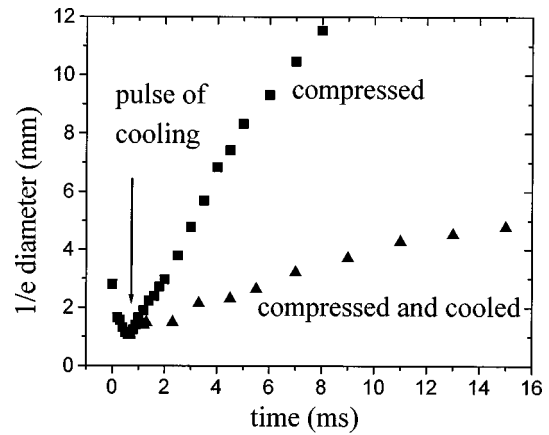


Fig. 8. Time dependence of size of the atomic cloud after the compression pulse is switched off without (■) and with (▲) cooling pulse that is applied at T_{focus} .

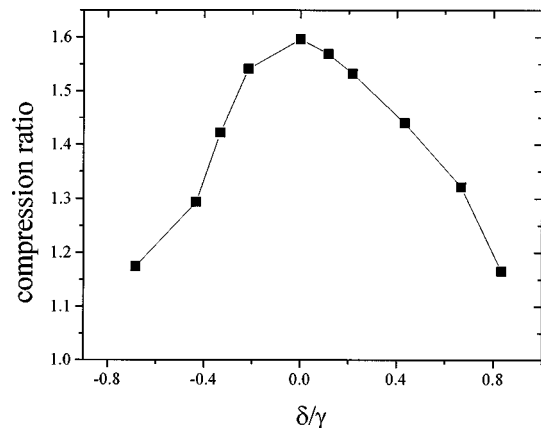


Fig. 9. Dependence of the two-beam compression ratio in quasi-steady-state realization on detuning of the compressed laser frequency from resonance. The symbols are our experimental data, and the connecting lines are only to guide the eye.

We compared the temperature of the atoms with and without the compression beam and observed no heating owing to compression beams. We also found that the compression was quite insensitive to the MOT beam parameters. Its sensitivity to the compression-beam intensity was similar to that of the pulse-compression case. Finally, we extended the 1-D quasi-steady-state compression into the 3-D case by using six compression beams (each overlapping one of the MOT beams) in the same temporal chopping sequence as in the two-beam case. Results nearly identical to those of the 1-D case were observed, in particular a maximal compression of $C = 1.5$. We attribute such a decrease in (quasi) steady-state compression in comparison with a pulsed scheme to a repulsive force, which is presented during a MOT operation, and possibly also to the presence of the MOT quadrupole magnetic field that stayed on continuously (unlike the pulsed scheme).

5. CONCLUSIONS

In summary, we analyzed the light-induced atom-atom interactions in an optically thick and cold atomic cloud

and found that for relatively strong and on-resonance laser light they change sign and become attractive. This is in contrast to the common experimental case in laser cooling, where such interactions are repulsive and thus tend to hinder high atomic densities. On the basis of our analysis we proposed and demonstrated a novel scheme to compress the atomic cloud using a short on-resonance laser pulse. We showed that owing to laser-beam attenuation the scattering force applied on the atoms by the compression beam decreases approximately linearly with distance (provided that the beam intensity is properly chosen). This results in a lenslike behavior for the atomic motion that yields a transient increase in the peak density at the focal time T_{focus} .

We implemented our new compression scheme with one-beam, two-beam, and six-beam configurations, yielding maximal compressions of 2.2, 3.5, and 4, respectively, in the atomic density. The one-beam configuration was used to ease comparison between experiment and theory, whereas the latter configurations yielded improved compressions. The cooling of the compressed cloud at the focus time was utilized where the original temperature was restored, and a $3\times$ increase in phase-space density was observed. Finally a (quasi) steady-state version for our compression scheme was also demonstrated, where either two or six (on-resonance) compression beams were temporally chopped with the (red-detuned) MOT beams. Only a moderate ($1.6\times$) increase in peak density was observed but without any observed heating or loss of atoms.

The compression scheme may be improved in several ways. First, the compression pulse can be made nonuniform (in space and/or in time) so as to reduce the spherical aberration of the focusing. Our simulations indicate that a $2\times$ increase in the compression ratio can be thereby achieved. Second, the six-beam configuration can be replaced by three consecutive two-beam configurations that are expected to yield higher compression ratios. Third, the compression may be applied to a quasi 1-D distribution of atoms, such as a one-beam dipole trap. For such configurations the scattered photons have a much smaller probability to be reabsorbed within the trap than for an isotropic configuration, and thus their repulsive (and heating) effects are further reduced.²²

The results presented in this paper can be utilized in two respects. Practically, they enable a transient increase in the density of cold atomic clouds in completely free space without any laser and magnetic fields. Alternatively, careful investigation of the dynamic of the cold and optically dense atomic cloud in the presence of a strong pump can yield more information on the light-induced atom-atom interaction. New effects such as amplification of spontaneous emission and photon localization can be observed and analyzed.²³

ACKNOWLEDGMENTS

We thank Nir Friedman and Roei Ozeri for helpful discussions and Rosty Bron for his assistance. This work was supported in part by the Minerva Foundation and the Israel Science Foundation. N. Davidson is an incumbent of the Rowland and Sylvia Schaefer career development chair.

REFERENCES AND NOTES

1. E. L. Raab, M. Prentiss, A. Cable, S. Chu, and D. E. Pritchard, "Trapping of neutral sodium atoms with radiation pressure," *Phys. Rev. Lett.* **59**, 2631 (1987).
2. See special issue on laser cooling and trapping of atoms, S. Chu and C. E. Wieman, eds., *J. Opt. Soc. Am. B* **6**, 2020 (1989).
3. D. Sesko, T. Walker, and C. Wieman, "Behavior of neutral atoms in a spontaneous force trap," *J. Opt. Soc. Am. B* **8**, 946 (1991).
4. J. Dalibard, "Laser cooling of an optically thick gas: the simplest radiation pressure trap?" *Opt. Commun.* **68**, 203 (1988).
5. A. P. Kazantsev, G. I. Surdutovich, D. O. Chudensnikov, and V. P. Yakovlev, "Scattering, velocity bunching, and self-localization of atoms in a light field," *J. Opt. Soc. Am. B* **6**, 2130 (1989).
6. W. Petrich, M. H. Anderson, J. R. Ensher, and E. A. Cornell, "Behavior of atoms in a compressed magneto-optical trap," *J. Opt. Soc. Am. B* **11**, 1332 (1994).
7. W. Ketterle, K. B. Davis, M. A. Joffe, A. Martin, and D. E. Pritchard, "High density of cold atoms in a dark spontaneous-force optical trap," *Phys. Rev. Lett.* **70**, 2253 (1993).
8. C. G. Townsend, N. H. Edwards, K. P. Zetie, C. J. Cooper, J. Rink, and C. J. Foot, "High-density trapping of cesium atoms in a dark magneto-optical trap," *Phys. Rev. A* **53**, 1702 (1996).
9. C. G. Townsend, N. H. Edwards, C. G. Cooper, K. P. Zetie, C. J. Foot, A. M. Steane, P. Szriftgiser, H. Perrin, and J. Dalibard, "Phase-space density in the magneto-optical trap," *Phys. Rev. A* **52**, 1423 (1995).
10. These changes also affect the spring constant, as shown by A. Steane, M. Chowdhury, and C. Foot, "Radiation force in the magneto-optical trap," *J. Opt. Soc. Am. B* **9**, 2142 (1992).
11. See, for instance, evaporative cooling in N. Masuhara, J. M. Doyle, J. C. Sandberg, D. Kleppner, T. J. Greytak, H. F. Hess, and G. P. Kochanski, "Evaporative cooling of spin-polarized atomic hydrogen," *Phys. Rev. Lett.* **61**, 935 (1988), or Raman cooling in H. J. Lee, C. S. Adams, M. Kasevich, and S. Chu, "Raman cooling of atoms in an optical dipole trap," *Phys. Rev. Lett.* **76**, 2658 (1996).
12. B. R. Mollow, "Power spectrum of light scattered by two-level system," *Phys. Rev.* **188**, 1969 (1969).
13. B. R. Mollow, "Stimulated emission and absorption near resonance for driven system," *Phys. Rev. A* **5**, 2217 (1972).
14. After scattering of a few photons, optical pumping aligns each atom with respect to the linearly polarized laser light. For this situation the saturation intensity for rubidium is $I_{\text{sat}} = 3 \text{ mW/cm}^2$ instead of 1.65 mW/cm^2 for a completely polarized atom. It is also nearly uniform among the three occupied m states. Throughout the paper we scale intensities to this I_{sat} despite different experimental situations.
15. We assume a uniform spatial distribution of the atoms over the period of the standing wave. This is applicable to the on-resonance case ($\delta = 0$), whereas at $\delta \neq 0$ some localization of the atoms toward the nodes ($\delta > 0$) and the antinodes ($\delta < 0$) of the standing wave is expected owing to the dipole force. We neglect this localization here.
16. A. Fioretti, A. F. Molisch, J. H. Müller, P. Verkerk, and M. Allegrini, "Observation of radiation trapping in a dense Cs magneto-optical trap," *Opt. Commun.* **149**, 415 (1998).
17. At low intensities the neglect of the repulsive inter-atomic forces by our simplified model is not justified anyway.
18. To calculate C_{average} , we extended the simulations to a two-dimensional Gaussian density distribution $n(x, y, z = 0)$, and the one-dimensional integrated density was defined as $\int n(x, y, z = 0) dy$, corresponding to our imaging fluorescence measurements that are described below.
19. P. D. Lett, R. N. Watts, C. I. Westbrook, W. D. Phillips, P. L. Gould, and H. J. Metcalf, "Observation of atoms laser cooled below the Doppler limit," *Phys. Rev. Lett.* **61**, 169 (1988).

20. We observed nearly identical dependence on laser detuning in one-beam and six-beam configurations.
21. Note that for the pulsed compression the optimal compression was obtained for detuning of 1–2 MHz above resonance (see inset of Fig. 7). This frequency shift can be explained by the fact that when the atoms are accelerated during the $\sim 100\text{-}\mu\text{s}$ compression pulses they acquire a negative Doppler shift of a few megahertz, so their average detuning is close to zero when their initial detuning is somewhat positive. This does not apply for the quasi steady state of Fig. 9, as is confirmed by the exact zero location of the optimal detuning.
22. D. Boiron, A. Michaud, J. M. Fournier, L. Simard, M. Sprenger, G. Grinberg, and C. Salomon, "Cold and dense cesium clouds in far-detuned dipole traps," *Phys. Rev. A* **57**, R4106 (1998).
23. L. Khaykovich, N. Friedman, and N. Davidson, "Saturation of the weak probe amplification in a strongly driven cold and dense atomic cloud," *Europhys. J.* (to be published).